Study of metal distributions in $YBa_2Cu_3O_{7-x}/Ag_2O$ composites

Study of metal distributions in YBa$_2$Cu$_3$O$_{7-x}$/Ag$_2$O composites

M Faiz†, M Ahmed‡, N M Hamdan†, Kh A Ziq† and J Shirokoff‡

† Department of Physics, King Fahd University of Petroleum and Minerals, Dhahran
‡ Research Institute, King Fahd University of Petroleum and Minerals, Dhahran
31261, Saudi Arabia

Abstract. The micro proton-induced x-ray emission technique has been used to study the elemental distribution profiles of YBa$_2$Cu$_3$O$_{7-x}$/Ag$_2$O high-T_c composites on varying the Ag$_2$O content. Measurements revealed that Ag agglomeration starts to appear in samples with $\geq$25 wt% Ag$_2$O, becoming prominent at 50 wt%. These results are further supported by x-ray diffraction (XRD) measurements performed on the same samples. The XRD results identified a crystalline Ag phase to be present in all of the samples (7–50 wt% Ag$_2$O), a crystalline Ag$_2$O phase in the 25 and 50 wt% Ag$_2$O samples and no evidence for Ag replacing Cu or orthogonal-to-tetragonal transformation.

1. Introduction

Practical applications of high-temperature superconductors (HTSCs) demand superb mechanical as well as superconducting properties. Mechanical properties of YBa$_2$Cu$_3$O$_{7-x}$ (Y123) are generally poor because of low ductility [1–3]. Although adding silver may slightly decrease the critical temperature, it increases the critical current density, reduces the normal-state resistivity [4] and improves the mechanical properties of HTSCs [5–8]. Silver has also been used as a cladding material for shaping HTSC ceramics into wires and tapes [7–9] and has been found to enhance crystal growth at the interface between grains of Bi2212 and Ag casing [10]. Grain boundaries of Y123 not only act as possible sources for mechanical failure but also are responsible for its low critical current density [11]. The addition of a small amount of Ag seems to enhance the grain growth of Y123 in Y123/Ag composites [12, 13] and to improve superconducting properties. However, as the Ag content increases, more Ag inclusions become interconnected and the grain growth kinetics slows down significantly [13]. It is of great practical importance to determine these critical Ag concentrations above which deteriorating effects become dominant. These effects can clearly be seen in micro proton-induced x-ray emission (PIXE) elemental composition analysis. The PIXE technique can provide information very rapidly on elemental distribution and concentrations with parts per million sensitivity. Only a few applications of PIXE for HTSC characterization have so far been reported in the literature [14–16]. In addition to average composition analysis, elemental distribution profiles can be very important in understanding microscopic variations in the properties of HTSC. These elemental distribution maps can be generated using a focused scanning proton microbeam [16]. In this study, samples of Y123 with different amounts of Ag$_2$O addition are analysed by the micro-PIXE and x-ray diffraction (XRD) techniques, in an effort to relate the effects of Ag$_2$O distribution and the superconducting properties of Y123/Ag$_2$O composites.

2. Experimental details

Y123 powder was prepared by solid-state reaction of the constituent oxides mixed in appropriate proportions. The Y123/Ag$_2$O composites were prepared by grinding various weight ratios of Ag$_2$O (99% purity) with high-quality polycrystalline YBa$_2$Cu$_3$O$_{6.9}$ ($T_c \sim$ 92 K, $\Delta T \sim$ 1 K) and sintering at 950 °C in an oxygen atmosphere for at least 18 h. The samples were cooled down to room temperature at a rate of 5–10 °C min^{-1} with intermediate annealing at 500–600 °C in an oxygen atmosphere. The grinding and annealing processes were repeated to ensure random distribution of the Ag$_2$O powder. In this way, Y123/Ag$_2$O composites with starting Ag$_2$O concentrations of 7, 10, 14, 25 and 50 wt% were obtained. The critical temperatures of these samples and pure Y123 (0 wt% Ag) were determined by a standard four-probe technique, using a constant-current source and a Keithly-181 nanovoltmeter. XRD patterns were obtained from the samples using a Phillips PW1700 automated diffractometer with monochromator and spinner operating. The diffraction patterns were generated on a vertical goniometer attached to a broad-focus x-ray tube with copper target energized to 40 kV and 40 mA. The analysis is computer assisted so that the interplanar spacing values can be corrected for the instrument error function by analysing a silicon standard and subsequent phase identification can be carried out. The samples were then
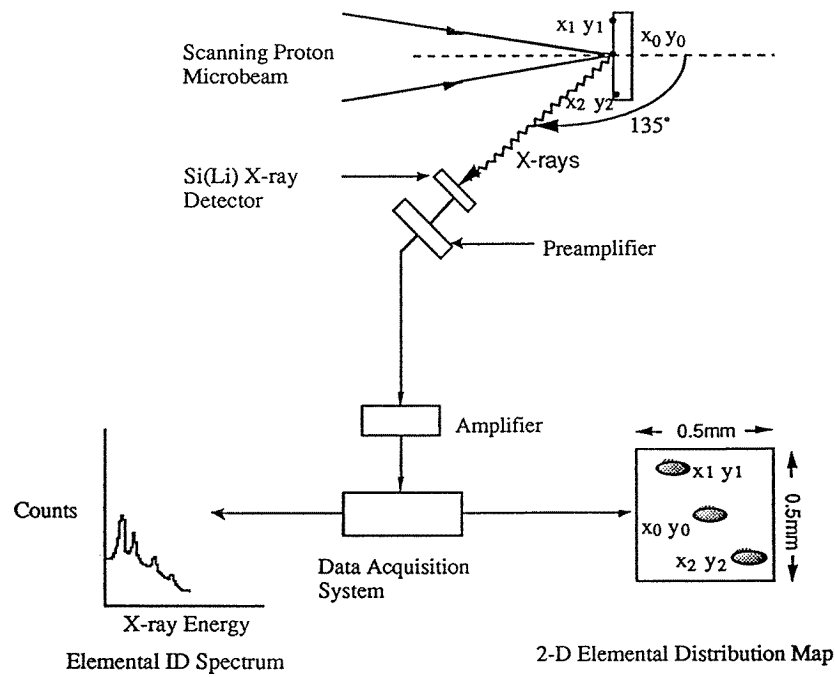
Figure 1. Schematic of the micro-PIXE setup.

analysed using the scanning microbeam facility available in the Tandetron Accelerator Laboratory at the Energy Resources Division of the Research Institute, KFUPM. A detailed description of the facility has been reported elsewhere [17]. The micro-PIXE setup is shown in figure 1. A 2.5 MeV focused proton beam of about 4 μm resolution was used to scan an area of 500 μm $\times$ 500 μm at a time on the sample surface. The microbeam current was kept low (typically about 30 pA) to avoid any damage due to heating up of the sample. From each scanned area, an average elemental composition spectrum and several two-dimensional elemental distribution maps were acquired simultaneously.

3. Results and discussion

The samples used in this investigation were first characterized by monitoring their resistance as a function of temperature using a four-point contact method. Samples with $\leq$14 wt% Ag$_2$O have a zero-resistance transition temperature above 90 K. For samples with >14 wt% Ag$_2$O, the transition temperature dropped rapidly and the transition width increased with increasing Ag$_2$O content. The variation of the zero-resistance transition temperature with Ag$_2$O content is shown in figure 2.

The XRD patterns for all the samples, shown in figure 3, confirm that they are all single phase with orthorhombic symmetry. Further XRD indexing and refinement was performed using the Powder Diffraction Package (PDP) program [18]. The lattice parameters show very little deviation from those of the standard pure Y123 orthorhombic cell. The observed variations in the lattice parameters with Ag content are shown in figure 4. These variations reflect different residual stress
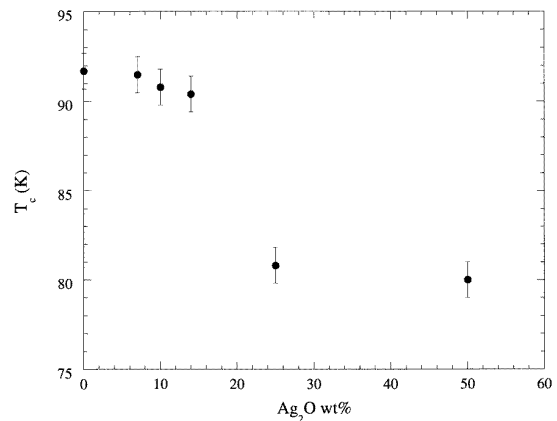

Figure 2. Variation of T_c with Ag$_2$O content.

values as a result of silver oxide addition [19]. The observed decrease in T_c with Ag$_2$O addition, seen in figure 2, may be caused by the change in residual stress, oxygen content and disorder in the oxygen sublattice. In addition, in Y123/Ag$_2$O composites, superconductor–metal–superconductor Josephson junctions formed by the Ag agglomeration (discussed later) between Y123 grains may also affect the value of transition temperature at zero resistance. This is supported by the long tail of resistivity versus temperature curve observed in 25 and 50 wt% Ag$_2$O samples [4, 20]. For all composite samples the XRD patterns clearly identify two Ag peaks, (200) and (220) reflections, at $2\theta = 44.2°$ and $64.2°$ respectively, indicating the presence of Ag as a separate phase and not replacing the constituents of Y123 [4, 21]. Since the (111) reflection of Ag$_2$O, which is known to have the highest
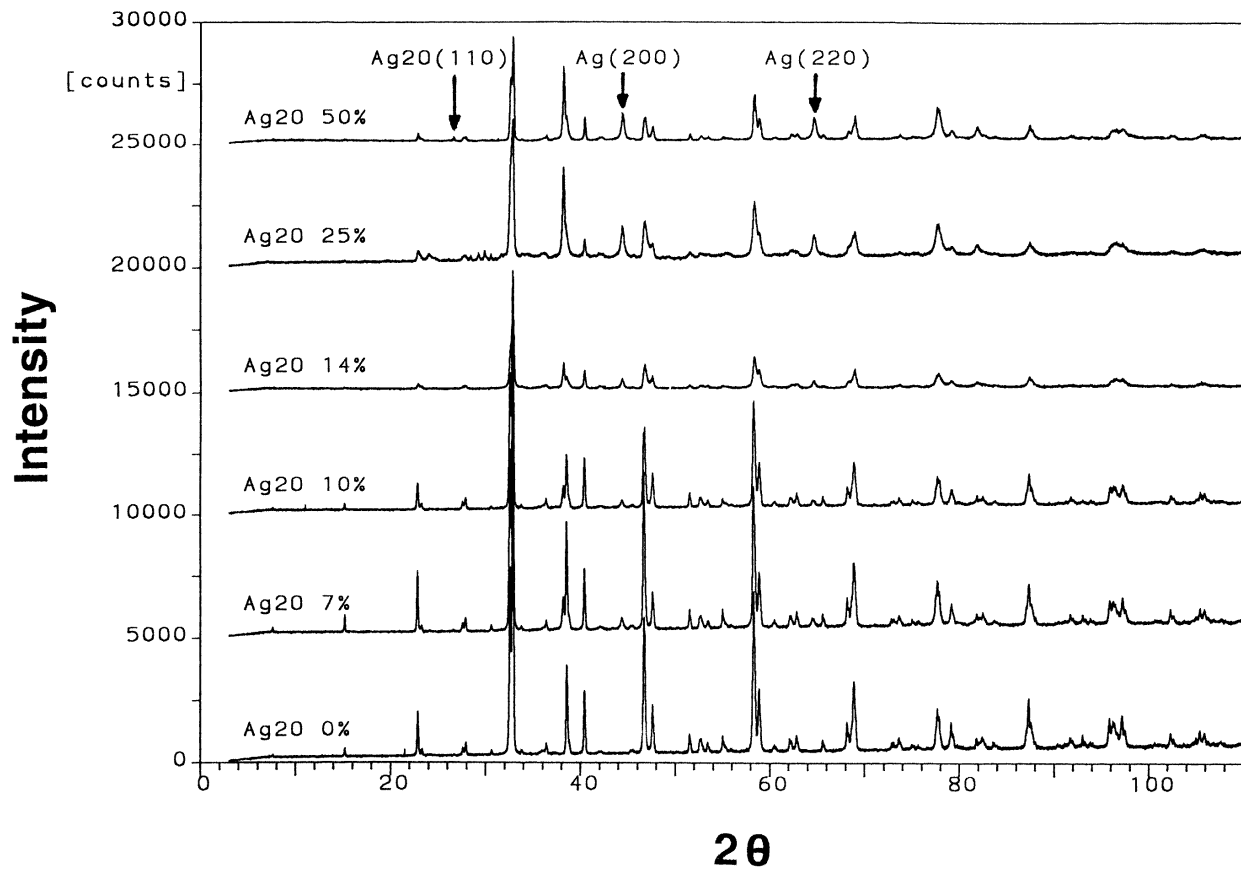
Figure 3. XRD patterns of Y123 with increasing amounts of Ag_2O. The x-ray patterns are vertically offset by 5000 counts from each other.

intensity, overlaps with the (103) and (111) reflections of Y123 orthorhombic cell, the (110) reflection of Ag_2O has been used to identify the Ag_2O phase. The (110) reflection of Ag_2O at $2\theta = 26.67°$ is clearly seen in the diffraction pattern of the sample with 50 wt% Ag_2O, indicating that the excess silver oxide remains in a separate phase and has not been decomposed to Ag and O. Nevertheless, a trace of the (110) reflection of Ag_2O ($I_{25}/I_{50} < 0.25$) is observed in the 25 wt% Ag_2O sample.

Silver addition affects superconducting and magnetic properties, such as critical current density J_c and pinning force. Recently, it has been found that scaling of pinning force continues up to about 14 wt% of Ag_2O. Above such Ag concentrations, gradual deterioration of magnetic and scaling behaviour has been observed [22]. The sample with 50 wt% Ag_2O is drastically degraded.

To look at the distributions of Ag and other elements in the composite samples, we performed micro-PIXE analysis. Figure 5 shows a typical x-ray energy spectrum for the sample with 50 wt% Ag_2O showing traces of Cr and Fe, estimated to be at ppm level, as impurities which might have originated from the Ag_2O. Note that XRD did not detect these impurities because of the very low concentrations. Figure 6 shows the Ag distribution maps for all six samples. It can be seen from the distribution maps that Ag is uniformly distributed in samples with Ag_2O up to
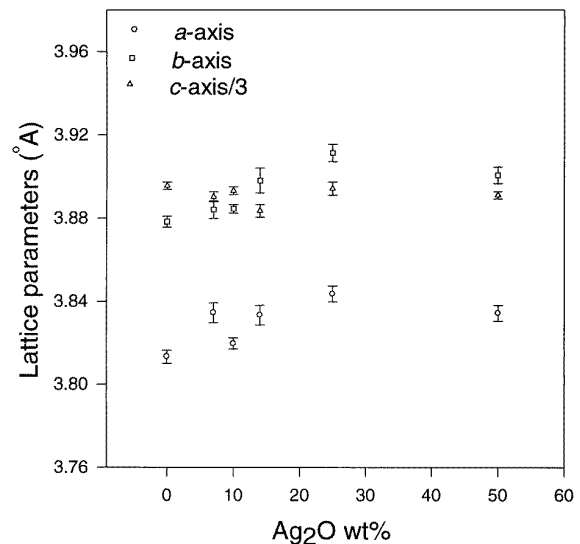

Figure 4. Variation of lattice parameters of Y123 with Ag_2O content.

14 wt%. Agglomeration starts to appear in the sample with 25 wt% Ag_2O, becoming most prominent in the 50 wt% Ag_2O sample. These results not only are consistent with the
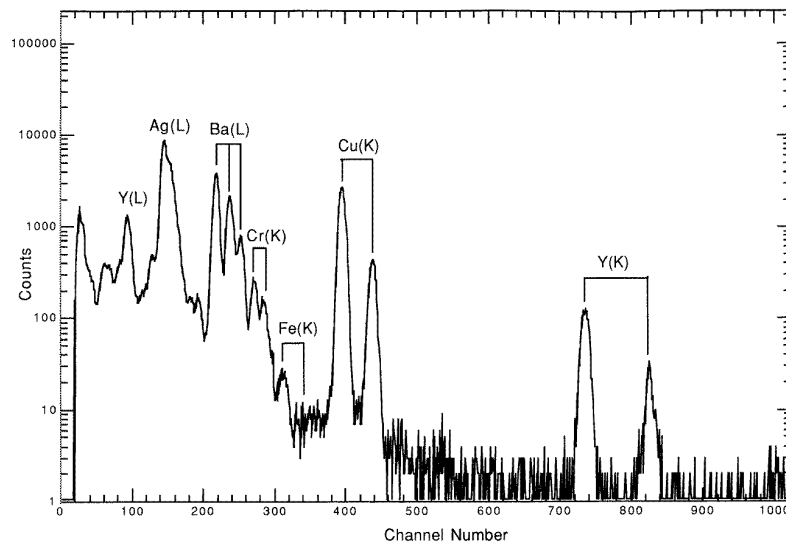
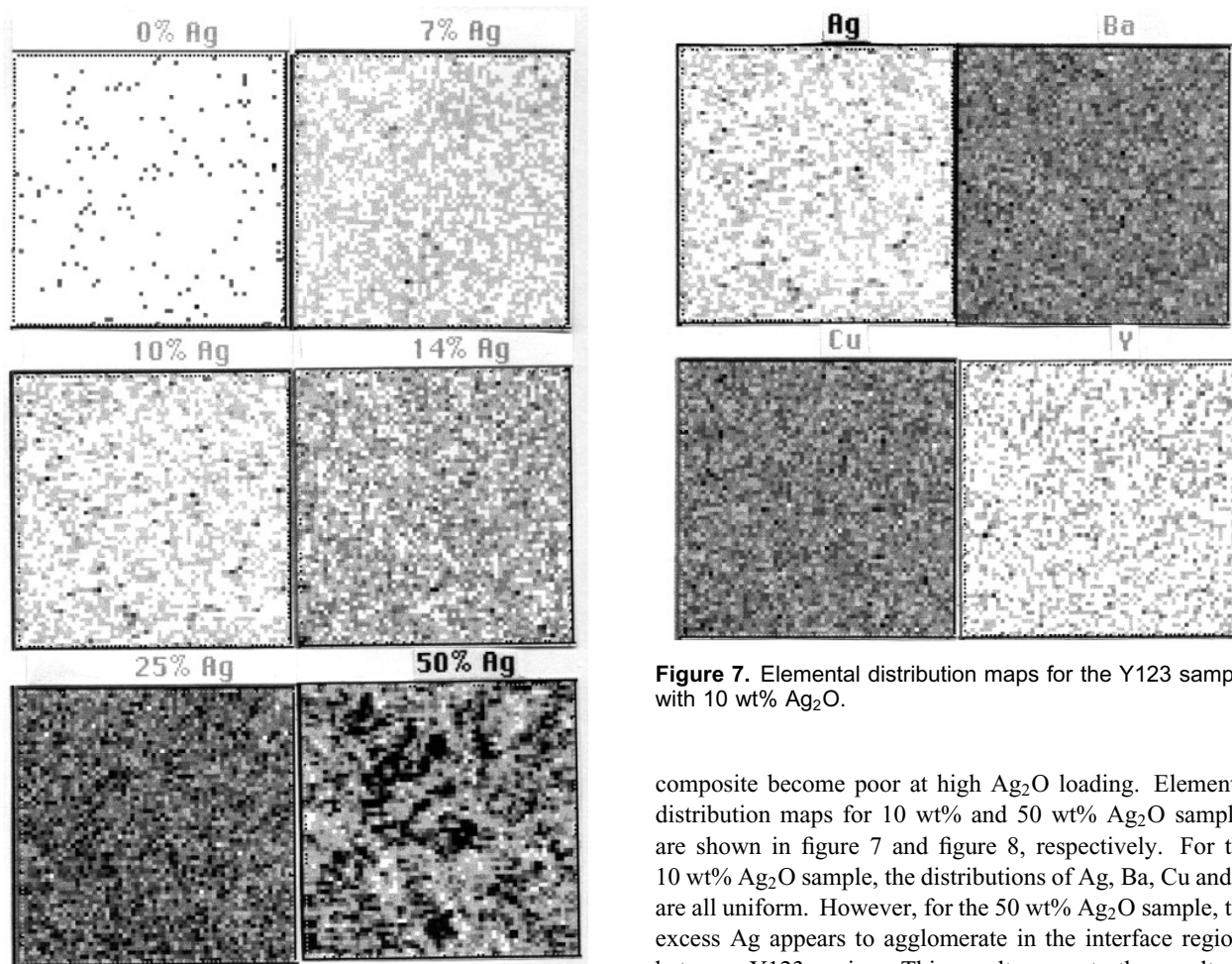**Figure 5.** A typical PIXE spectrum for the Y123 sample with 50 wt% Ag$_2$O.

Figure 6. Ag distribution maps for the Y123/Ag$_2$O composites.

observations mentioned earlier but also help to explain why superconducting and magnetic properties of Y123/Ag$_2$O

Figure 7. Elemental distribution maps for the Y123 sample with 10 wt% Ag$_2$O.

composite become poor at high Ag$_2$O loading. Elemental distribution maps for 10 wt% and 50 wt% Ag$_2$O samples are shown in figure 7 and figure 8, respectively. For the 10 wt% Ag$_2$O sample, the distributions of Ag, Ba, Cu and Y are all uniform. However, for the 50 wt% Ag$_2$O sample, the excess Ag appears to agglomerate in the interface regions between Y123 grains. This result supports the results of Tuan and Wu [13], mentioned in section 1. The above results are consistent with our XRD observations that Ag exists as a separate phase in all samples prepared with Ag$_2$O precursor and Ag$_2$O phase in the samples with 25 and 50 wt% Ag$_2$O.
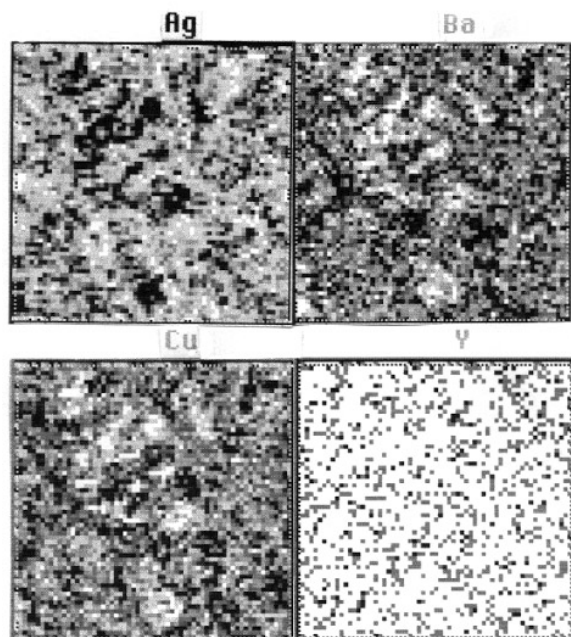
Figure 8. Elemental distribution maps for the Y123 sample with 50 wt% Ag_2O.

4. Conclusion

In summary, our micro-PIXE results show that Ag agglomeration starts to appear in the 25 wt% Ag_2O sample and it is most prominent when Ag_2O is increased to 50 wt%, which segregates the Y123 grains. This might contribute to the deterioration of certain superconducting and magnetic properties of these composites above 14 wt% Ag_2O loading. These findings are consistent with the XRD results from the Y123/Ag_2O composites which reveal (i) no evidence for Ag replacing Cu in the Y123 phase, (ii) a crystalline Ag phase to be present in all of the samples prepared with Ag_2O, (iii) a crystalline Ag_2O phase to be present in the 25 and 50 wt% Ag_2O samples and (iv) no indication of orthogonal-to-tetragonal structural phase transition occurring.

Acknowledgments

References

[1] Cook R F, Dinger T R and Clark D R 1987 *Appl. Phys. Lett.* **51** 454

[2] Cook R F, Shaw T M and Duncombe P R 1987 *Adv. Ceram. Mater.* **2** 606

[3] Alford McN, Birchall J D, Clegg W J, Harmer M A, Kendall K and Jones D H 1988 *J. Mater. Sci.* **23** 761

[4] Abdelhadi M 1993 *MS Thesis* Department of Physics, King Fahd University of Petroleum and Minerals

[5] Pavuna D, Berger H, Tholence J L, Affronte M, Sanjines R, Dubas A, Bugnon P and Vasey F 1988 *Physica* C **153–155** 1339

[6] Singh J P, Shi D and Capone D W 1988 *Appl. Phys. Lett.* **53** 237

[7] Matsumuro A, Kasumi K, Mizutani U and Senoo M 1991 *J. Mater. Sci.* **26** 737

[8] Ozkan H, Albiss B A, Hamdan N and Menerad A 1994 *J. Supercond.* **7** 885

[9] Zannella S, Martini L, Ottobani V, Parmigiani F, Ricca A M and Ripamonti G 1989 *Physica* C **162–164** 1179

[10] Finnemore D K, Ming Xu, Kouzoudis D, Bloomer T, Kramer J, Mckernan S, Balachandran U and Haldar P 1996 *Appl. Phys. Lett.* **68** 556

[11] Clarke D R, Shaw T M and Dimos D 1989 *J. Amer. Ceram. Soc.* **72** 1103

[12] Tiefel T H, Jin S, Sherwood R C, David M E, Kammlott G W, Gallagher P K, Johnson D W Jr, Fastnacht R A and Rhodes W W 1989 *Mater. Lett.* **7** 363

[13] Tuan W H and Wu J M 1993 *J. Mater. Sci.* **28** 1409

[14] Ishii A and Nakamura K 1993 *Nucl. Instrum. Methods* B **75** 388

[15] Sandrik R 1994 *Nucl. Instrum. Methods* B **85** 154

[16] Faiz M, Ahmed M and Al-Ohali M A 1996 *Nucl. Instrum. Methods* B **114** 138

[17] Ahmed M, Nickel J, Hallak A, Abdel-Aal R, Coban A, Al-Juwair H and Aldaous M 1993 *Nucl. Instrum. Methods* B **82** 584

[18] Calligaris M and Gevemia S 1990 Department of Chemistry, University of Trieste, personal communication

[19] Ziq Kh A, Hamdan N M and Shirokoff J 1994 *Physica* C **235–240** 1217

[20] Dubson M A, Herbert S T, Calabrese J J, Harris D C, Patton B R and Garland J C 1988 *Phys. Rev. Lett.* **60** 1061

[21] Ganapathi L, Kumar A and Narayan J 1990 *Mater. Res. Soc. Symp. Proc.* **169** 1267

[22] Hafidh E A 1996 *MS Thesis* Department of Physics, King Fahd University of Petroleum and Minerals and references therein